ARL-TR-9310 ● SEP 2021

DEVCOM ARMY RESEARCH LABORATORY

Enhanced Human Identification in the Thermal Infrared Using Mid-IR and Longwave-IR Polarimetric Imaging

by Kristan P Gurton

NOTICES

Disclaimers

The findings in this report are not to be construed as an official Department of the Army position unless so designated by other authorized documents.

Citation of manufacturer's or trade names does not constitute an official endorsement or approval of the use thereof.

Destroy this report when it is no longer needed. Do not return it to the originator.

ARL-TR-9310 ● SEP 2021

Enhanced Human Identification in the Thermal Infrared Using Mid-IR and Longwave-IR Polarimetric Imaging

Kristan P Gurton
Computational and Information Sciences Directorate,
DEVCOM Army Research Laboratory

REPORT DOCUMENTATION PAGE

Form Approved
OMB No. 0704-0188

1. REPORT DATE *(DD-MM-YYYY)*	2. REPORT TYPE	3. DATES COVERED (From - To)
September 2021	Technical Report	1 April–30 June 2021

4. TITLE AND SUBTITLE
Enhanced Human Identification in the Thermal Infrared Using Mid-IR and Longwave-IR Polarimetric Imaging

5a. CONTRACT NUMBER

5b. GRANT NUMBER

5c. PROGRAM ELEMENT NUMBER

6. AUTHOR(S)
Kristan P Gurton

5d. PROJECT NUMBER

5e. TASK NUMBER

5f. WORK UNIT NUMBER

7. PERFORMING ORGANIZATION NAME(S) AND ADDRESS(ES)
DEVCOM Army Research Laboratory
ATTN: FCDD-RLC-ES
Adelphi, MD 20783-1138

8. PERFORMING ORGANIZATION REPORT NUMBER
ARL-TR-9310

9. SPONSORING/MONITORING AGENCY NAME(S) AND ADDRESS(ES)

10. SPONSOR/MONITOR'S ACRONYM(S)

11. SPONSOR/MONITOR'S REPORT NUMBER(S)

12. DISTRIBUTION/AVAILABILITY STATEMENT
Approved for public release: distribution unlimited.

13. SUPPLEMENTARY NOTES

14. ABSTRACT
Until very recently, facial recognition techniques relied on data sets that were predominately derived using visible imagery that often required a degree of ambient illumination while being recorded. However, there are applications in which human identification is required in environments devoid of any form of visible light or illumination (e.g., nighttime observation). Under such circumstances, IR thermal imaging is usually applied for target location and identification, but was considered insufficient for human identification applications since conventional thermal imagery lacks the detailed spatial information required for face recognition. Reported here are results of ongoing research that involves a new form of thermal imaging that takes advantage of additional polarization-state information inherent in most image forming radiation (i.e., polarimetric thermal imaging). By creating thermal image sets based solely on polarization-state information, we show significant improvement in the spatial detail displayed in the resultant thermal imagery for both mid-IR and longwave IR spectral wavebands.

15. SUBJECT TERMS
thermal polarimetric, mid-infrared, MidIR, longwave-infrared, LWIR, face recognition, human identification, thermal imaging

16. SECURITY CLASSIFICATION OF:			17. LIMITATION OF ABSTRACT	18. NUMBER OF PAGES	19a. NAME OF RESPONSIBLE PERSON
a. REPORT	b. ABSTRACT	c. THIS PAGE			Kristan P Gurton
Unclassified	Unclassified	Unclassified	UU	41	19b. TELEPHONE NUMBER (Include area code) (301) 394-2093

Contents

List of Figures

List of Tables

1. Introduction

Face recognition has been an active area of research for several decades, given its wide range of potential applications in commercial, military, and government sectors. However, face recognition research has been focused primarily in the visible region of the electromagnetic (EM) spectrum. Recently, researchers have developed methods for face recognition in the infrared (IR) spectrum, particularly in near-IR (NIR) (i.e., 0.74–1 μm wavelength), shortwave IR (SWIR) (1–3 μm wavelength), and thermal IR, to a limited extent. Facial signatures acquired in the NIR and SWIR bands are more similar to the visible spectrum facial signature, while facial signatures collected in the thermal IR band appear significantly different from their visible spectrum counterparts. Unfortunately, imagery derived in the visible, NIR, and SWIR rely to varying degrees on ambient illumination, either manmade or naturally occurring. As a result the ability to identify a particular individual using visible, NIR, and SWIR, imagery is greatly limited, if not impossible, when the test subject is poorly illuminated.

Alternatively, imagery recorded in thermal IR do not experience such limitations, since it predominately based on thermal emission rather than reflection of ambient light. In general, the thermal IR portion of the spectrum is composed of two waveband regions (i.e., the mid-IR [MidIR] at 3–5 μm wavelength and longwave-IR [LWIR] at 8–14 μm wavelength). Although, imaging in the thermal IR does not rely on ambient illumination, the resultant image of a human face (either in MidIR or LWIR) is often described as being "ghost-like", devoid of the detailed spatial features often exhibited in visible imagery (Fig. 1).

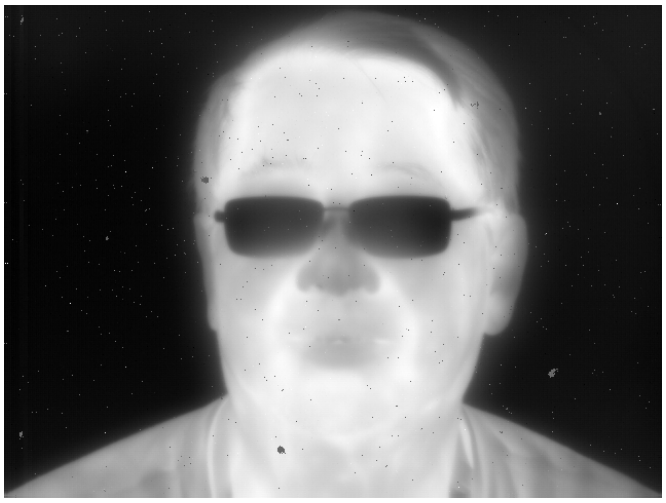

Fig. 1 Conventional LWIR thermal image. Shown is the typical "ghosting" effect inherent in both MidIR and LWIR imagery.

However, over the past decade, there has been much research designed to develop a new type of thermal camera system capable of optically filtering the image-forming radiance that forms a scene based on the polarization state. These type of imaging systems are often termed "polarimetric imagers" and exist for both and MidIR and LWIR operation.[1–4]

Polarimetric sensors that operate in the thermal IR are designed to exploit the phenomena that "manmade" objects tend to emit thermal radiation that has a preferential linear polarization state, while naturally occurring "background" materials (e.g., vegetation, grass, trees, and so on) tend to show little or no preferential linear polarization. As a result, a thermal polarimetric image can significantly enhance the ability to detect certain objects hidden by background clutter or that exhibit poor thermal contrast (i.e., a low-observable). Examples of such application include the detection of improvised explosive devices (IEDs) or buried landmines, enhanced targeting and tracking of manmade vehicles and personnel, the identification and suppression of military decoys, and improved remote detection of hidden or camouflaged targets.[5–8]

Because a thermal polarimetric image contains both conventional thermal and polarization information, when augmented, the resultant scene tends to display much more detail compared to the conventional thermal image only. As an example, Fig. 2 shows a conventional LWIR thermal image (left) and the resultant polarimetric degree-of-linear-polarization (DoLP) image (right).

Fig. 2 LWIR thermal (left) and the resultant polarimetric DoLP image (right) comparison of a Russian 1970s vintage T-72 tank

Only recently has thermal polarimetric imaging been applied to face recognition applications. A particular focus of face recognition research has involved cross-spectrum, or heterogeneous, face recognition algorithm development. The objective of cross-spectrum face recognition is to recognize the identity of an individual imaged in one spectral band (e.g., thermal) from a gallery database

containing face imagery acquired in another band (e.g., a visible spectrum database). For cross-spectrum face recognition, the gallery is usually taken to be in the visible spectrum, since real-world biometric databases and watch lists are typically only made up of visible imagery. Given the similar reflective phenomenology in the visible, NIR, and SWIR bands, research on NIR-to-visible face recognition[1,2] and SWIR-to-visible face recognition[3,4] has achieved some measure of success. However, thermal-to-visible face recognition is significantly more challenging due to the difference in phenomenology between the thermal and visible spectra. Recently, several research groups[5–8] have developed techniques for and evaluated the performance of thermal-to-visible face recognition, achieving limited success. Although thermal-to-visible face recognition is highly challenging, it is also highly desirable as thermal imaging is often used to provide enhanced situational awareness for environments in which ambient illumination is not present (e.g., nighttime surveillance).

Until now, all prior research in the area of face recognition using thermal imagery has been limited to image sets recorded in the LWIR.[9–16] Fortunately, new MidIR polarimetric camera systems have been developed by Polaris Sensor Technologies Inc. (Huntsville, Alabama) that have been explicitly designed for human ID applications.

Prior efforts involving the LWIR had reported differences in the quality of polarimetric facial imagery depending on whether it was recorded outside or indoors within a laboratory setting. Specifically, facial polarimetric images recorded indoors exhibited a reduction in recorded linear polarization on the order 8%–12%, compared to outside image capture. This reduction in recorded linear polarization was attributed to increased levels of ambient LWIR radiation present within an enclosed room due to thermal emission from the walls and ceiling. In comparison, ambient radiant levels outside, in the LWIR, are significantly lower because the thermal background under clear sky conditions exhibits radiance levels typically associated with blackbody temperatures well below 0 °C, often referred to as “cold sky” conditions.

To better understand this effect in the thermal IR, a study was conducted in which polarimetric imagery of facial profiles were recorded in both the LWIR and MidIR, under varying conditions and temperatures, to better quantify this phenomena. Objects imaged were both an actual human test subject and a set manikin heads. The manikin head surfaces were coated with either a smooth mirror-like pigment or a diffuse carbon-black polymer in an attempt to produce surfaces that were highly reflective or emissive in thermal IR.

2. MidIR and LWIR Polarimetric Sensors

For this test, two thermal polarimetric sensors were considered, each functioning in either the MidIR or LWIR region of the spectrum. Both systems were acquired from Polaris Sensor Technologies Inc. (Huntsville, Alabama). The LWIR system image capture system is based on a Stirling cooled, mercury cadmium telluride (MCT) focal-plane array (FPA) with a pixel density of 640 × 480, while the MidIR platform utilized "two" indium antimonide (InSb) FPAs, each with pixel densities of 1280 × 1024; however, each polarimetric camera used a different optical configuration to accomplish the necessary polarimetric filtering. Specifically, the LWIR polarimetric camera was based on a spinning-achromatic-retarder (SAR) design, while the MidIR platform used a two-camera, division-of-amplitude (DoA), SAR hybrid optical configuration.[17–19]

An image of the Stirling cooled LWIR SAR polarimetric camera in shown in Fig. 3, which uses a rapidly spinning achromatic phase retarder mounted in series with a linear polarizer. A "sequence" of images are recorded at a 120-Hz frame rate, where each image represents a particular polarization state. A Fourier modulation technique is applied to the pixel readout in which a Fourier series expansion is calculated for each channel. Finally, the expansion is inverted to yield the Stokes image parameters in terms of Fourier coefficients. This LWIR polarimetric system was equipped with a dual-focus objective (i.e., 45- and 145-mm optic) resulting in either a near or far field of view (FOV) of 10.6° × 7.9° and 3.3° × 2.5°, respectively. Additional key parameters are shown in the Table 1.

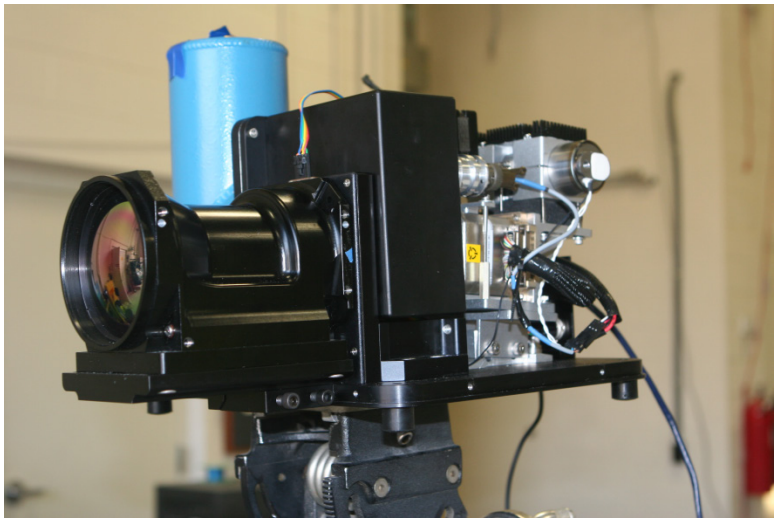

Fig. 3 LWIR MCT polarimetric camera system based on the SAR design

Table 1 Technical parameters for the LWIR SAR-based polarimetric camera system

Parameter	Specification
Format	640 × 480
Waveband	7.5–11.1 μm
Pixel size	15-μm square
NEΔT	25 mK at f/2
NEΔDoLP	0.1%
Frame rate	120 Hz
Dynamic range	14-bit
Narrow FOV	3.3° × 2.5°
Wide FOV	10.6° × 7.9°
Pixel size	15 × 15 μm
Instantaneous FOV (IFOV) at 1 km	(Narrow FOV) 4 inches (Wide FOV) 12 inches

The polarimetric filtering architecture used for the MidIR sensor is a DoA SAR hybrid system that captures two orthogonal states by splitting the scene using a polarimetric beam splitting cube. Each state is projected onto one of the two InSb FPAs. The image forming radiance enters the system and passes through a half-wave achromatic retarder. The vertically polarized radiance emerging from the half-wave retarder is transmitted through the polarizing beam splitter cube, while the horizontally polarized radiance is reflected off the hypotenuse face of the polarizing beam splitter cube.

When the system is operated, the half-wave retarder is rotated continuously. During the integration time, the retarder sweeps through a finite range of angles depending on the integration time and frame rate. For example, if a 4-ms integration time is chosen with a 60-Hz frame rate, then the retarder sweeps through an angle of $(4 \times 10 - 3 \cdot 60 \cdot 22.5° = 5.40)$. The intensity modulation caused by the rotation of the half-wave retarder is reduced by a small amount of 0.8%. For most operations, the integration time is approximately 7 ms. As a result, the polarization contrast is not impacted by the continuous rotation of the retarder. The MidIR system was specifically designed for long-range applications and can be equipped with either a 600-mm objective (long range) or a 25-mm objective (short range). Pictures of the MidIR DoA SAR hybrid system with the 600- and 25-mm objectives mounted, are shown in Fig. 4a and b, and the key parameters of the MidIR system are shown in Table 2.

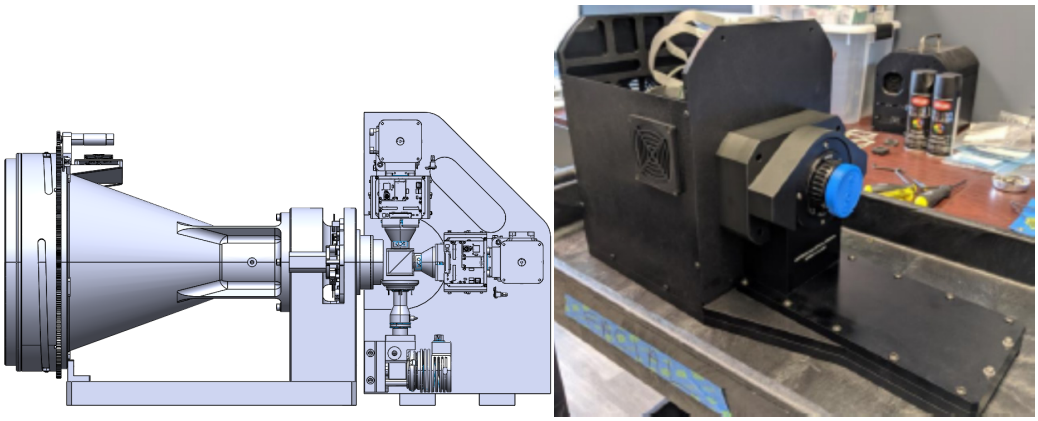

a b

Fig. 4 a) Cross section of the MidIR polarimeter with the long-range objective mounted, and b) 25-mm objective mounted

Table 2 Key parameters for the MidIR DoA-SAR hybrid polarimetric sensor

Parameter	Value
Detector	InSb 2D array
Waveband	3.7–4.8 µm
Resolution (H x V)	1280 × 1024 pixels
Pixel Pitch	10 µm
EFL	600 mm, 25 mm
F/#	3
Horizontal FOV	1.22° (600 mm), 28.72° (25 mm)
IFOV	16.8 µRad (600 mm), 396.6 µRad (25 mm)
Frame Rate	50 Hz
Focus	Motorized (600 mm), Manual (25 mm)
Bit Depth	13 bit
NEDT	28 mK
NEDoLP	0.14%
Size (L x W x H)	25.5x10x13.5 inches (600 mm), 22.8x10x13.5 inches (25 mm)
Weight	60 lbs (600 mm), 45 lbs (25 mm)
Input Power Supply	24 VDC @ 10 A
Data Interface	USB 3.0

3. Polarimetric Methodology

For polarimetric applications, it is common practice to use a Stokes parameter approach to describe the polarization state of the image forming radiation that results from either emission or reflection.[20] We apply the Stokes parameter methodology to our imaging application, where we define the Stokes parameters images S1, S2, and S0 by Eqs. 1–3,

$$S1 = I(0) - I(90) \quad (w/sr\text{-}cm^2), \quad (1)$$

$$S2 = I(+45) - I(-45) \quad (w/sr\text{-}cm^2), \quad (2)$$

$$S0 = \text{total calibrated radiance image} \quad (w/sr\text{-}cm^2), \quad (3)$$

and the DoLP is defined as

$$\text{DoLP} = \frac{\sqrt{S1^2 + S2^2}}{S0}, \tag{4}$$

where I(0), I(90), I(+45), and I(-45) represent 2-D LWIR images produced with polarimetrically filtered radiance polarized (relative to the vertical plane) at 0°, 90°, +45°, or –45°, respectively. As one can see from Eqs. 1–3, the S1 image represents a measure of the vertical as compared to the horizontal state, the S2 image represents a measure of the difference between the two ±45° diagonal states, and the combined radiance image, S0, is taken to be equivalent to the conventional LWIR thermal image. Finally, it is common practice to normalize S1 and S2 with respect to S0 in order to generate unitless fraction (i.e., S1(%) = 100 × (S1/S0) and S2(%) = 100 × (S2/S0)) and this is the convention we use throughout this report.

4. Emission- versus Refection-Induced Polarization

Because we are comparing the detection response between two different IR wave-band regions, it is informative to understand how linear polarization states, induced by either "reflection" or "emission", combine at the sensor to yield the *net* polarimetric response.

Typically, thermal radiation in the thermal IR either becomes linearly polarized by reflection from the surface of an object or becomes polarized when thermal energy is emitted from the surface of an object. Induced polarization due to either reflection or emission arise from the fact that both parameters are directionally dependent quantities (i.e., $\rho(\lambda, \theta, \phi)$ and $\varepsilon(\lambda, T, \theta, \phi)$), where ρ and ε are the directional reflection and emission coefficients, respectively; and θ and ϕ are directions defined relative the object's surface normal, $\hat{n}$. As a result, the values of these quantities change depending on how they are viewed. Taking these formulations into account, one can rewrite each quantity in terms of a superposition of orthogonal components as shown in Eqs. 5 and 6:

$$\rho(\lambda, \theta, \phi) = \frac{\rho_{\perp}(\lambda,\theta) + \rho_{\parallel}(\lambda,\theta)}{2} \qquad \text{Total reflectivity} \tag{5}$$

$$\varepsilon(\lambda, T, \theta, \phi) = \frac{\varepsilon_{\perp}(\lambda,T,\theta) + \varepsilon_{\parallel}(\lambda,T,\theta)}{2} \qquad \text{Total emissivity} \tag{6}$$

As a result, the DoLP due to reflection, $DoLP_{\rho}$ and emission, $DoLP_{\varepsilon}$ can be expressed in Eqs. 7 and 8:

$$DoLP_{\rho} = \frac{(\rho_{\perp}(\lambda,\theta) - \rho_{\parallel}(\lambda,\theta)}{(\rho_{\perp}(\lambda,\theta) + \rho_{\parallel}(\lambda,\theta)} \qquad \text{Reflection-induced polarization} \qquad (7)$$

$$DoLP_{\varepsilon} = \frac{(\varepsilon_{\perp}(\lambda,\theta) - \varepsilon_{\parallel}(\lambda,\theta)}{(\varepsilon_{\perp}(\lambda,\theta) + \varepsilon_{\parallel}(\lambda,\theta)} \qquad \text{Emission-induced polarization} \qquad (8)$$

Although not apparent from the scalar Eqs. 7 and 8, Fresnel theory predicts the DoLP due to reflection, $DoLP_{\rho}$, is *orthogonal* with respect to the DoLP due to emission, $DoLP_{\varepsilon}$.[21]

As a result, when an object exhibits both types of induced polarizations, the *net* total DoLP, $DoLP_{Total}$, recorded by a polarimetric sensor represents a vector superposition of the two orthogonal states, which combine to reduce the net measured linear polarization response and is given by Eq. 9:

$$DoLP_{Total} = \left| DoLP_{\rho} - DoLP_{\varepsilon} \right| \qquad \text{“net” polarization state} \qquad (9)$$

Figure 5 presents a visual representation showing how induced polarization due to both reflected thermal radiation and thermal emission combine at the sensor, resulting in a net reduction of received linear polarization.

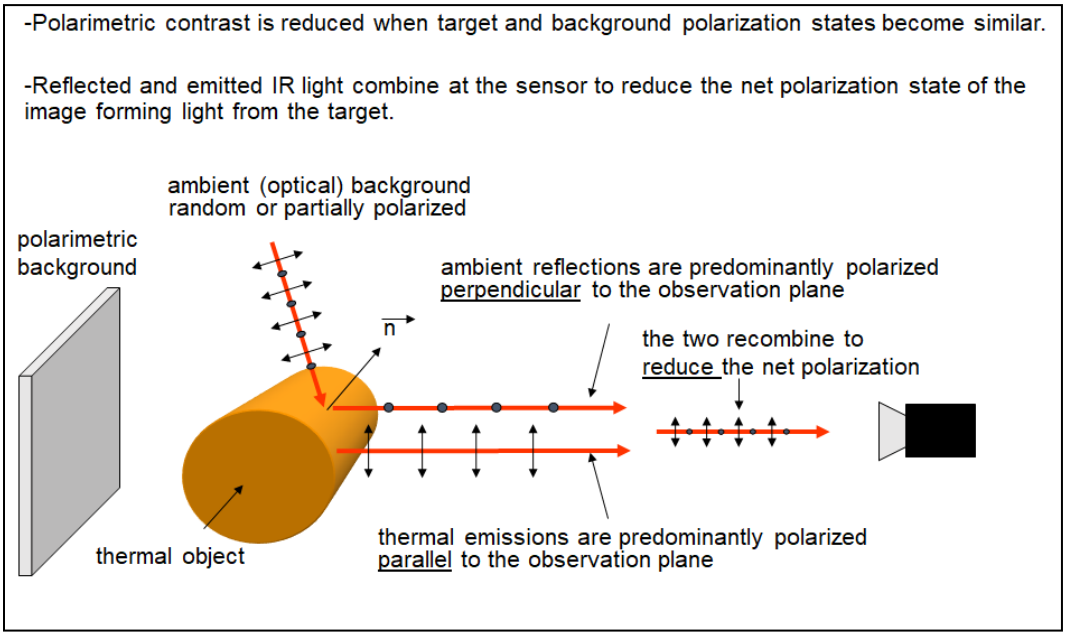

Fig. 5 Schematic showing how recorded linear polarization state is reduced by the superposition of induced polarized radiance that results from both emission and reflected energy

In practice, one type of induced polarization is usually dominate, which serves to define the direction and magnitude of resultant measureable DoLP signal. In addition, it is not uncommon to see polarization states “flip”, as evident in the sign

of either S1 or S2 for environments in which ambient conditions are changing (e.g., changing cloud cover or effects due to the daily diurnal cycle).[22]

5. Polarimetric Image Capture

Polarimetric imagery and video was recorded over multiple sessions using both the LWIR and MidIR camera systems described in Section 2. Test subjects (human and manikin heads) were imaged in either an inside or outdoor setting. The inside setting was intentionally chosen to maximize ambient radiant effects. This was done by placing the subject in a small hallway in which floor, walls, and ceilings where approximately 2 m from the image test point. Conversely, the outside test scenario was chosen to minimize ambient radiant effects. Test subjects were positioned in an open setting in which sky conditions were clear and devoid of any cloud cover (i.e., often referred to as "cold sky" conditions).

Before image capture, both sensors underwent a nonuniformity-correction (NUC) procedure in which know radiance from a calibrated extended blackbody is directed into each camera in order to flood-fill the imaging objective. This allows for direct conversion from camera raw signal "counts" into integrated absolute radiance values (w/sr-cm^2).

Test subjects consisted of either an actual human head (body temperature 36 °C), or a pair of manikin heads that were coated with either a diffuse carbon-black pigment or a highly reflective "mirror"-like epoxy resin (Fig. 6). Coatings for the manikin heads were chosen to represent either an "emission" or "reflective" dominate target based on being coated with the carbon-black or mirror epoxy coatings, respectively. It should be noted that the thermal response for the carbon-black manikin is expected to be very similar to what has be measured in prior studies involving actual human test subjects since the emissivity for carbon-black paint and human skin are $\varepsilon = 0.97$ and $\varepsilon = 0.98$, respectively.[23]

Fig. 6 Image of coated diffuse carbon-black manikin head (left) and coated mirror pigment manikin head (right) used as "emissive" and "reflective" targets, respectively

The first test conducted was to determine temperature dependencies on the polarimetric images, S1, S2, and DoLP for both MidIR and LWIR spectral band, under conditions of ambient radiant loading (i.e., recorded indoors). Manikin heads were artificially heated above the ambient room temperature of 21 °C, to a maximum temperature of approximately 50 °C, using a conventional laboratory heat-gun. Imagery was recorded with each camera operating at 30 frames/s and a 20-frame average was generated for the radiant image S0, the two Stokes images S1 and S2, and polarimetric product image DoLP. The resultant set of four images formed cube, and a representative region of interest (ROI) was chosen and projected to all images. Pixel average values were then generated for all four images. Resultant values for S1, S2, and DoLP (represented as a linear polarization percentage) are shown in Fig. 7, and the recorded radiant values S0 (units watt/cm^2*sr) are displayed separately in Fig. 8.

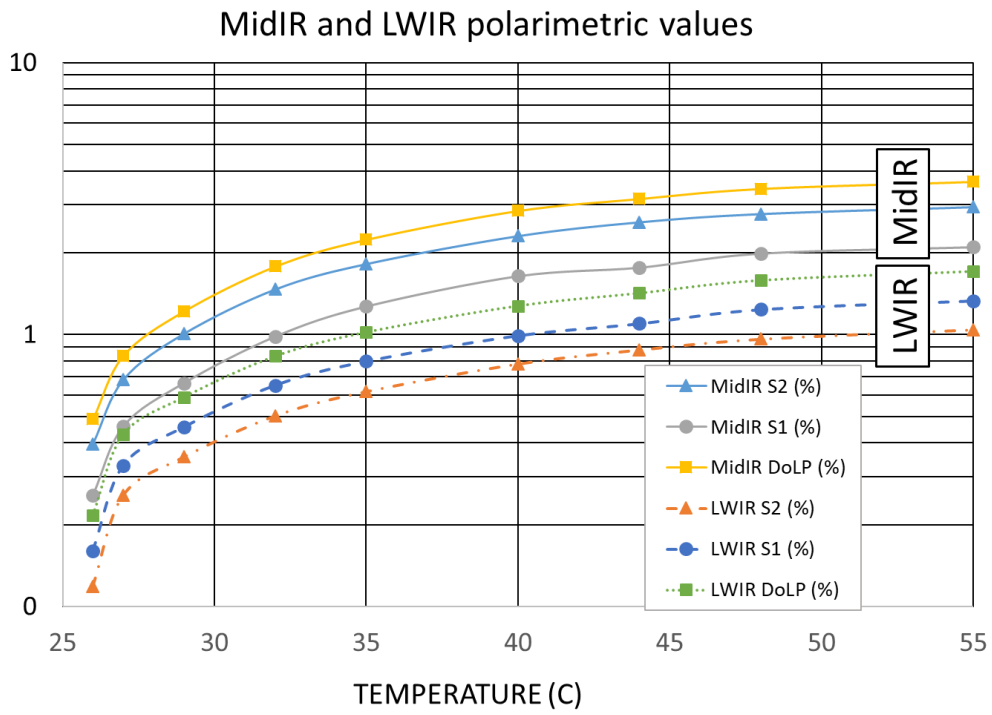

Fig. 7 Plot of polarimetric values S1, S2, and DoLP as a function of temperature for both MidIR and LWIR imagery

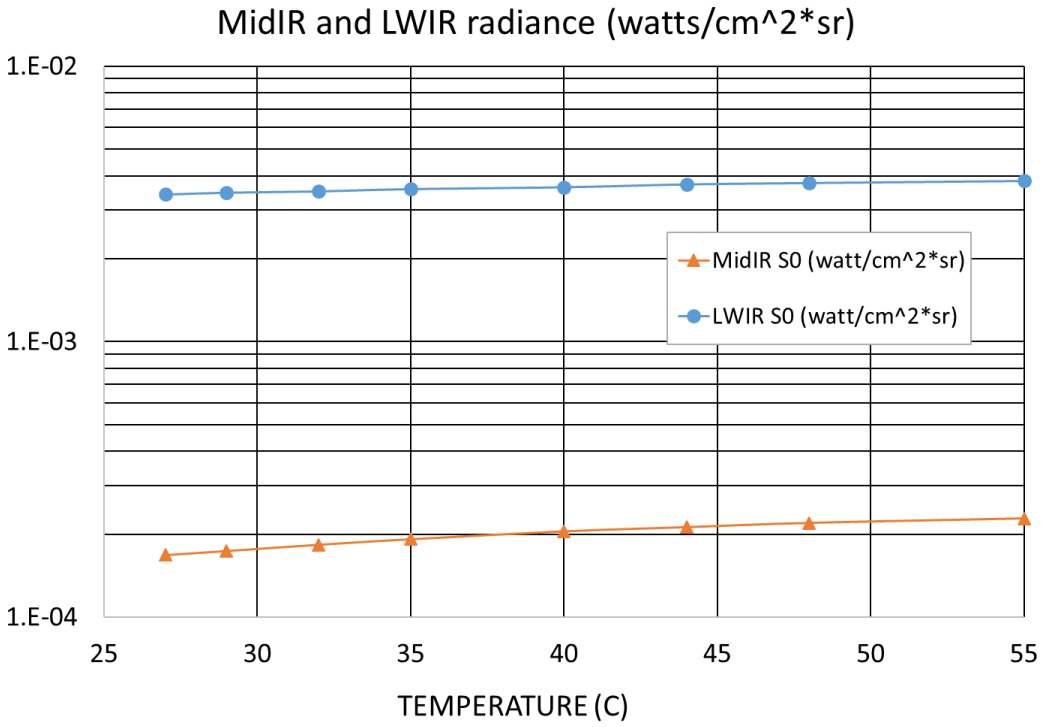

Fig. 8 Plot of measured thermal radiance values S0 (watt/cm^2*sr) as a function of temperature for both MidIR and LWIR imagery

As seen in Fig. 7, the measured DoLP for all polarimetric images is constantly higher in the MidIR portion of the spectrum compared to the LWIR, although the received magnitude of the thermal radiance in the MidIR is approximately an order of magnitude less (see Fig. 8). At first glance, one might think this to be counterintuitive, until the effect of ambient loading is considered. To gain some perspective, Planck calculations were conducted from 2 to 14 µm for temperatures 20 and 40 °C (Fig. 9).

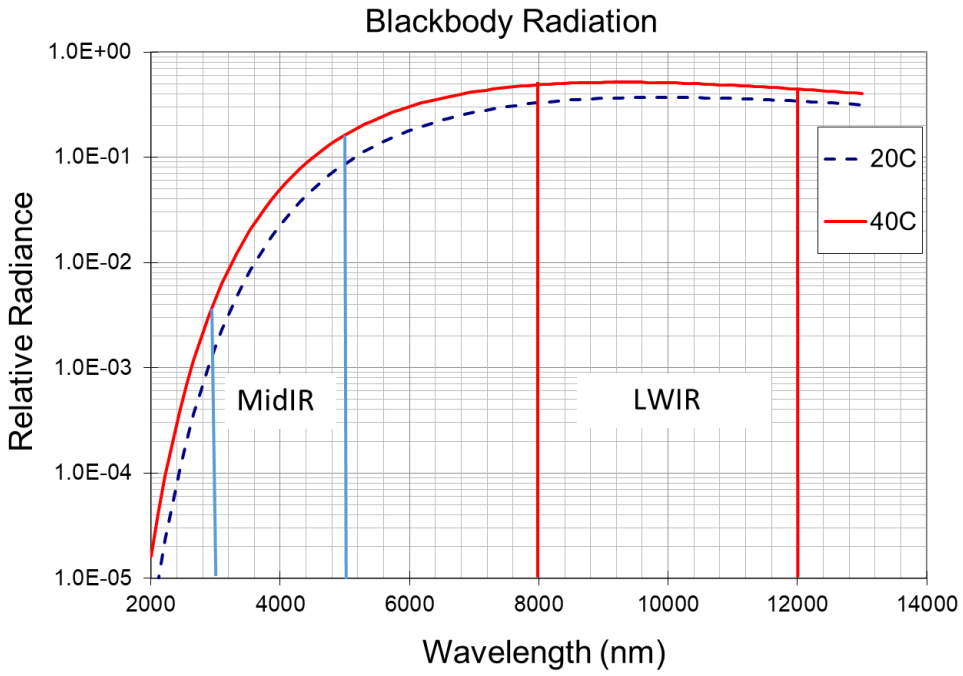

Fig. 9 Plank calculation from 2–14 µm for a typical blackbody at 20 and 40 °C

Figure 9 shows the relative radiant values for a typical blackbody (i.e., emissivity value 1) in both 3–5-µm (MidIR) and 8–12-µm (LWIR) ranges. Here we assume the hallway in which the imagery was recorded is made up of materials with emissivity values in the range 0.80–0.90.[24] As one can see, the ambient levels of relative radiance emitted by a hallway (temperature 20 °C) at 4 µm (center of MidIR band) is 2.19E-2 while at 10 µm (center of LWIR band) is 3.71E-1, or more than an order of magnitude higher. If one takes into account the effects described in Section 4 (i.e., reflected ambient radiance induces a polarization state orthogonal to emission induces polarization, resulting in a reduction in the measure polarization), then "less" ambient radiance in the MidIR results in "less" suppression of emission induce polarization, which leads to a "higher" measured DoLP value in the MidIR.

The next step was to offer a side-by-side comparison of the resultant images recorded by both cameras under varying conditions. Although this form of analysis

is somewhat subjective, it is still a valuable means of gaining insight to the relative polarimetric performance in each thermal band. In an attempt to offer some quantifiably measureable quantities such and maximum and minimum radiance and polarization quantities, ROIs required for analysis were again chosen based on the circumference of the facial region for each manikin (Fig. 10).

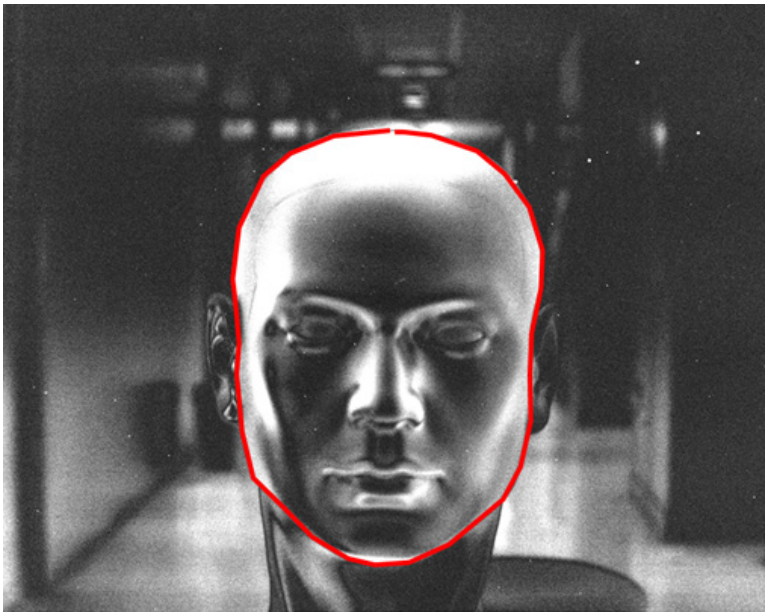

Fig. 10 Defined ROI used in analysis

The first scenario consider was to determine the effects ambient loading have on both the radiant, S0, and DoLP images for highly reflective and emissive surfaced targets. Imagery were recorded with targets at an ambient temperature of 23 °C and at 35 °C to mimic human body temperature. Figure 11 shows the LWIR image set for the reflective and emissive manikin heads at room temperature 23 °C. Also shown below each image are the minimum and maximum pixel values for S0 and DoLP for the ROI shown in Fig. 10. Similarly, Fig. 12 displays a similar set; however, now manikin heads are imaged at 35 °C.

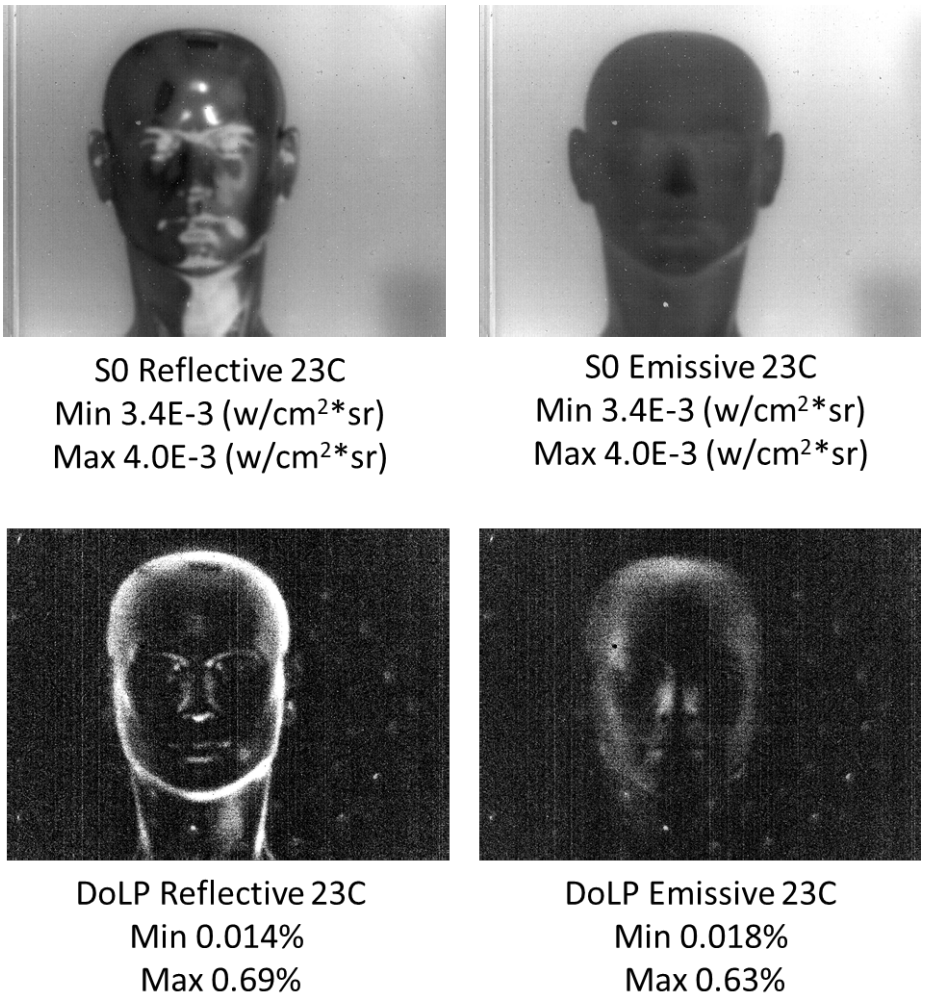

Fig. 11 LWIR image set at T = 23 °C of S0 and DoLP recorded in an environment in which there is radiant ambient illumination (i.e., recorded indoors). Displayed below each image is the target temperature and minimum and maximum pixel values for S0 and DoLP based on the ROI shown in Fig. 10.

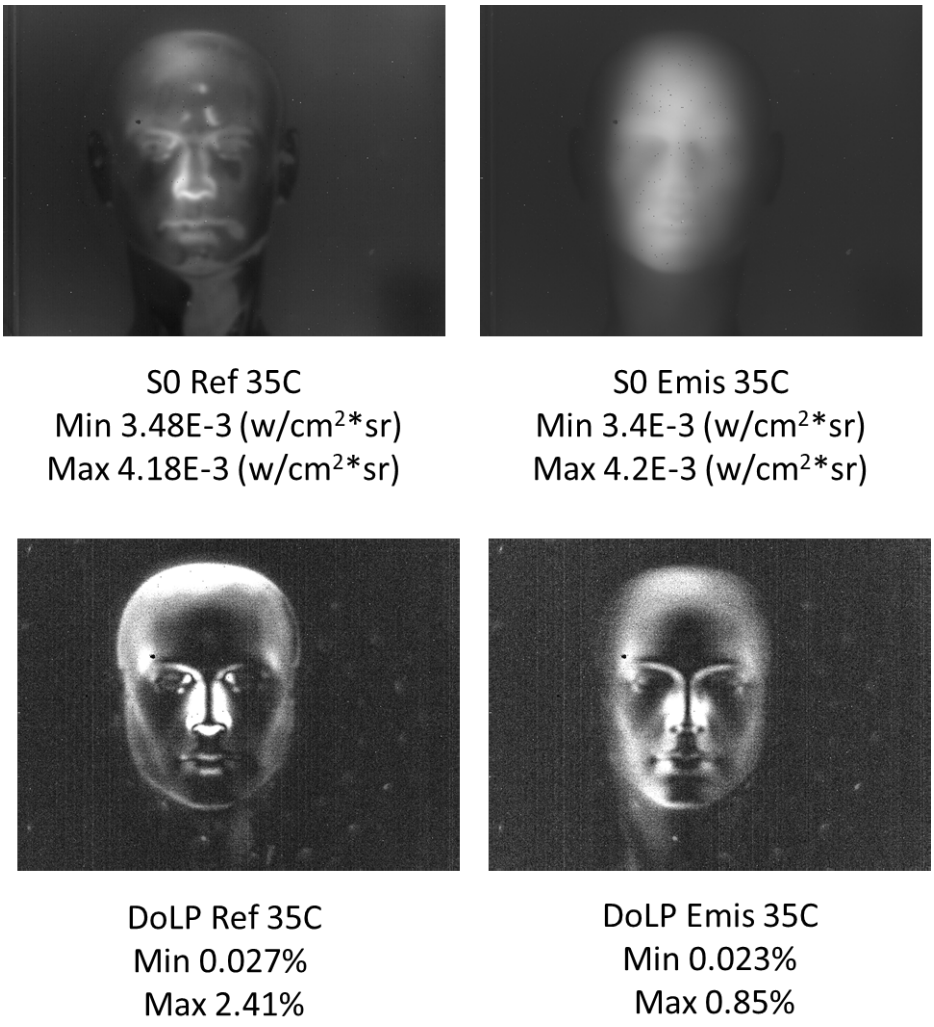

Fig. 12 LWIR image set at T = 35 °C of S0 and DoLP recorded in an environment in which there is radiant ambient illumination (i.e., recorded indoors). Displayed below each image is the target temperature and minimum and maximum pixel values for S0 and DoLP based on the ROI shown in Fig. 10.

Shown in both Figs. 11 and 12 is that the conventional LWIR radiant images, S0, show significant variance between the reflective and emissive manikins at both T = 23 °C and 35 °C. It is apparent the reflective coating produced a thermal image similar to what is seen in a conventional visible image (i.e., displaying detailed facial features) and is particularly apparent for the low-temperature manikin in which the majority of the image forming radiance is due to reflection of the ambient background. However, these features begin to fade for both the S0 and DoLP images as the manikin is heated and thermal emission begins to dominate over the reflected component of ambient background. Note that although the reflective nature of this manikin appears to exhibit certain facial features that are easily recognizable to a human observer, the highly reflective surface also produces a

strange shadowing anomaly due to reflections of the background and may result in poor performance when used as a bases set in a facial recognition algorithm.

In contrast, the emissive manikin, which most accurately mimics the response of a human face, shows moderate to significant improvement (compared to the LWIR radiant image S0) in displaying fine detailed facial features in the both DoLP images at T = 23 °C and 35 °C, respectively. Comparison of the DoLP images at T = 23 °C and 35 °C highlight the effect that ambient radiance has on suppressing the received polarimetric signal. At ambient temperature 23 °C, the levels of the reflective and emissive components of the polarization are comparable and orthogonal, thus reducing the net DoLP recorded. As the temperature rises, emission-induced polarization begins to dominate, and as a result, more surface detail become apparent. The apparently large DoLP value of 2.41% for the reflective manikin at T = 35 °C is attributed ultra-smooth finish that the reflective epoxy resin produced. It is well known that induced polarization is highly depended on surface roughness, where smoother surfaces tend to produce higher degrees of linear polarization compared to diffuse surfaces.[25]

A similar image set is shown in Figs. 13 and 14, where the test manikins are now imaged in the MidIR spectral region. It is interesting to note the behavior in S0 and DoLP for the reflective manikin as the temperature rises to 35 °C. At these temperatures, the reflective component of S0 and the DoLP image appears far more subdued resulting in a more uniform display of the facial details. Again, we attribute the unusually high DoLP value of 16.23% due to the ultra-smooth surface that resulted when coating the manikin with the reflective epoxy.

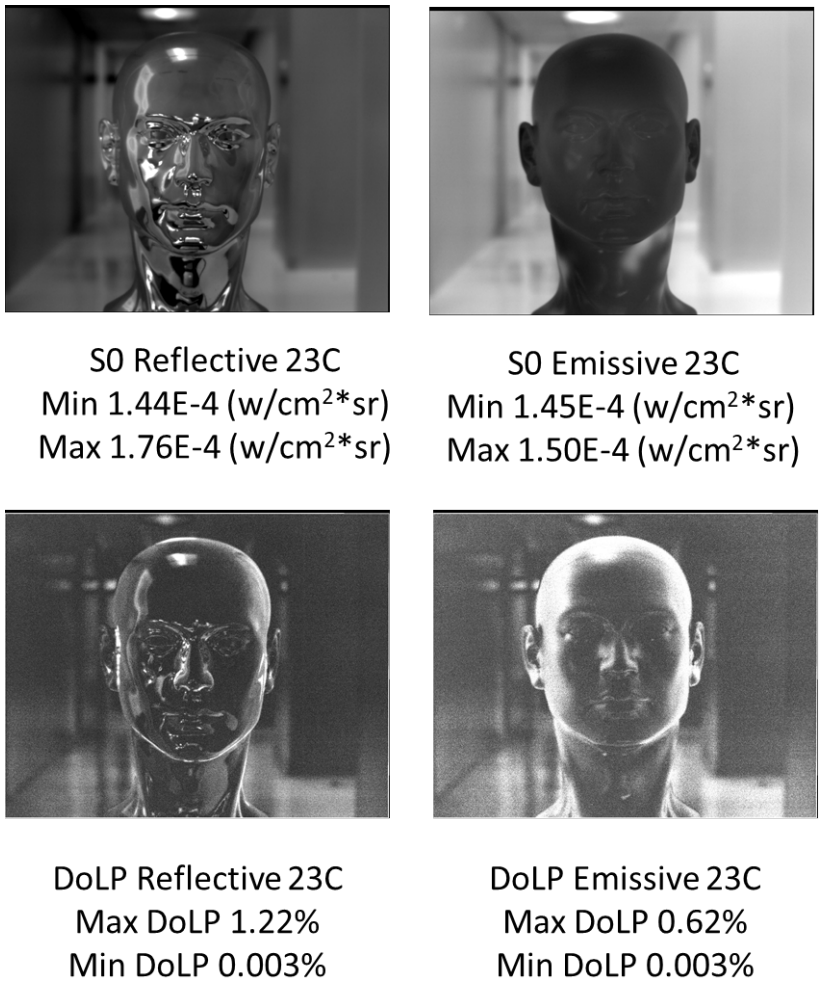

Fig. 13 MidIR image set at T = 23 °C of S0 and DoLP recorded in an environment in which there is radiant ambient illumination (i.e., recorded indoors). Displayed below each image is the target temperature and minimum and maximum pixel values for S0 and DoLP based on the ROI shown in Fig. 10.

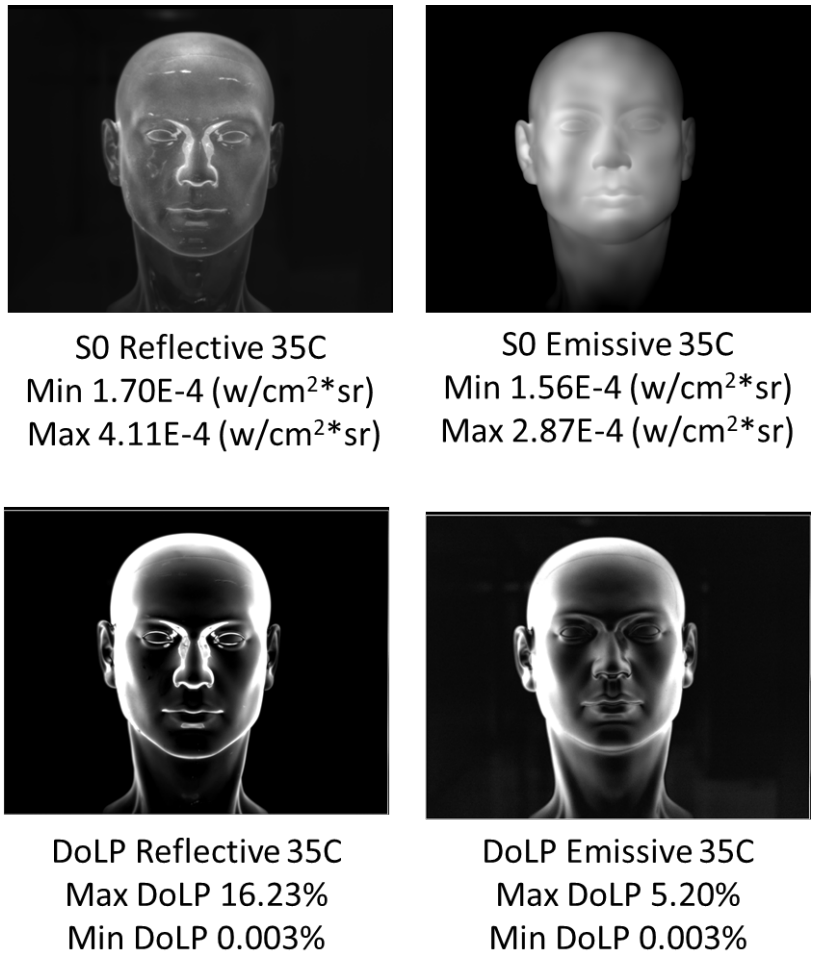

Fig. 14 MidIR image set at T = 35 °C of S0 and DoLP recorded in an environment in which there is radiant ambient illumination (i.e., recorded indoors). Displayed below each image is the target temperature and minimum and maximum pixel values for S0 and DoLP based on the ROI shown in Fig. 10.

After a qualitative review of all thermal images shown in Figs. 11–14, the emissive DoLP image at T = 35 °C (recorded in MidIR) "appears" to give the best representation of a "visible" image of the manikin head. However, it is very important to take into account the technological and performance differences between the two polarimetric camera systems before making such judgement. For example, the LWIR SAR system was built approximately 6 years earlier than the MidIR DoA-SAR hybrid system, and as result, the newer MidIR camera benefited greatly due to new technologies and improved design features. Perhaps most important to take into account when comparing relative performance between the two platforms are the difference between the FPAs used in each camera (e.g., focal-plane pixel density: MCT (LWIR) 640 × 480 vs. InSb (MidIR) 1280 × 1024).

Nevertheless, when much of these differences are taken into account, I am impressed with how robust polarimetric imaging appears for the MidIR

polarimetric sensor. This is particularly impressive since the test scenarios considered here should favor operation in the LWIR (i.e., target temperatures in the range 20–40 °C). Fortunately, there are efforts underway to develop dual-band MidIR/LWIR polarimetric imaging platforms that will utilize the same architecture and make polarimetric comparison between the two spectral bands much more straightforward.

The manikin heads were finally placed outside in an open environment in an effort to reduce effects due to ambient loading that resulted when targets were imaged inside. During the test, sky conditions were observed to be clear and devoid of cloud cover, but atmospheric conditions were unusually hot with a measured relative humidity of 78% and a measured temperature in the range of 36–37 °C (97–98 °F).

Unfortunately, our analysis was limited to the carbon-black-coated manikin head since the highly reflective manikin, when placed outside in the direct sunlight, produced overtly unnatural glare patterns of reflective radiance, and as result, was deemed unsuitable for analysis. Due to the hot temperatures experienced during the test, the carbon-black manikins acquired a temperature of 38 °C. Results for the emissive head are shown in Figs. 15 and 16 for the LWIR and MidIR image capture, respectively.

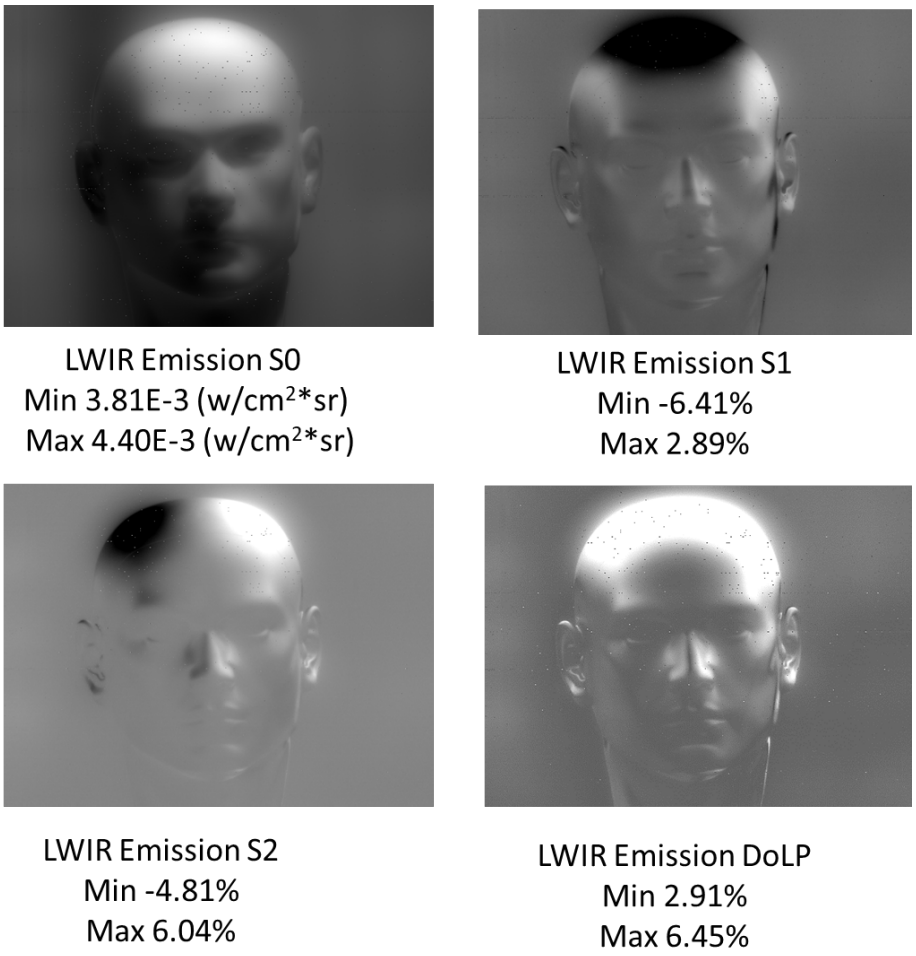

Fig. 15 LWIR image set recorded outside with manikin head at T = 38 °C. Shown are S0 and DoLP imagery recorded under clear sky conditions, with direct sunlight and a relative humidity 78%. Displayed below each image are minimum and maximum pixel values for S0 and DoLP based on a similar ROI as shown in Fig. 10.

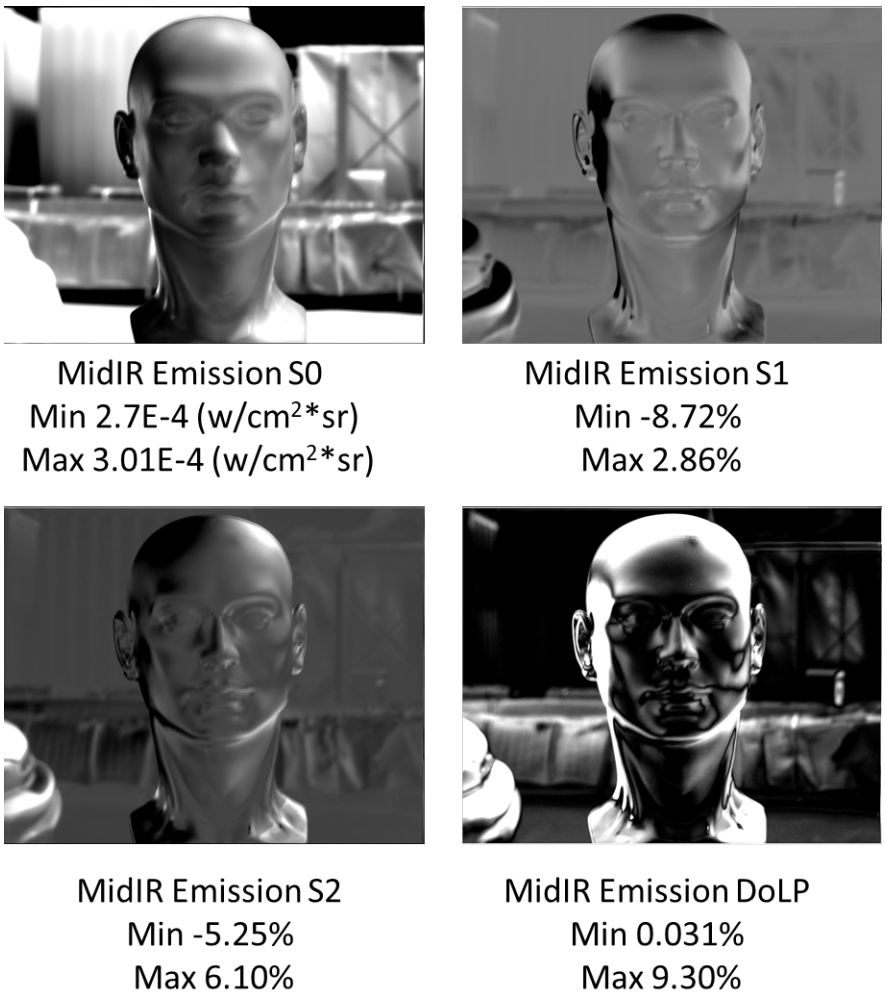

Fig. 16 MidIR image set recorded outside with manikin head at T = 38 °C. Shown are S0 and DoLP imagery recorded under clear sky conditions, with direct sunlight and a relative humidity 78%. Displayed below each image are minimum and maximum pixel values for S0 and DoLP based on a similar ROI as shown in Fig. 10.

Direct comparison between LWIR and MidIR images sets shown in Figs. 15 and 16 appears to show better performance for the MidIR set based on qualitative observations. In particular, the polarimetric performance seems superior in the MidIR for S1, S2, and the DoLP imagery, even when differences in FPA technology and spatial resolution between the two sensors are taken into account. Unfortunately, the performance of the LWIR system seemed unexpectedly poor. Appearance of the LWIR set were prone to intensity saturation effects were quite noticeable on the top of the forehead region, which resulted in the appearance of unusually low overall contrast. We believe this may be due to an unintended consequence of the high temperature of the manikin head due to exposure to direct sunlight, which resulted in a measured maximum radiance value of 4.40×10^{-3} w/sr-cm^2. Minimum and maximum temperatures chosen for the

"outside" NUC were 25 and 40 °C, and may have been insufficient for operation in the LWIR resulting in the apparent poor performance of the sensor.

For operation in the MidIR, intensity of the measured radiance was more than an order of magnitude less than in the LWIR, resulting in a maximum recorded radiance value of 3.01×10^{-4} w/sr-cm^2, compared to 4.40×10^{-3} w/sr-cm^2 shown in the LWIR S0 image. These elevated radiance levels produced maximum DoLP values of 6.45% and 9.30% for the MidIR and LWIR images, respectively.

The final portion of the study was to replace the manikins with an actual human subject and repeat the inside and outside test scenarios for both MidIR and LWIR polarimetric capture. Although study using manikins were informative, they cannot reproduce important human characteristics that result from differences in pigment and skin composition.[9,10]

Figures 17 and 18 show resultant image sets of a human subject at body temperature, 36 °C, recorded inside for both LWIR and MidIR operation, respectively. Figures 19 and 20 display a similar image set where the polarimetric imagery was recorded outside under the same atmospheric conditions as described above.

The comparison of the LWIR and MidIR image sets recorded indoors for human subject exhibits similar characteristics as seen for the manikin set shown in Figs. 14 and 15, in which recorded radiance in the MidIR band is lower by an order of magnitude, and conversely the DoLP is significantly higher in MidIR (i.e., maximum DoLP 0.93% in the LWIR compared to 2.90% seen in the MidIR). Again, the suppressed measured DoLP in both LWIR sets for human and manikin are attributed to the superposition of orthogonal components of polarization induced by reflection and emission from the subject, as described in Section 4.

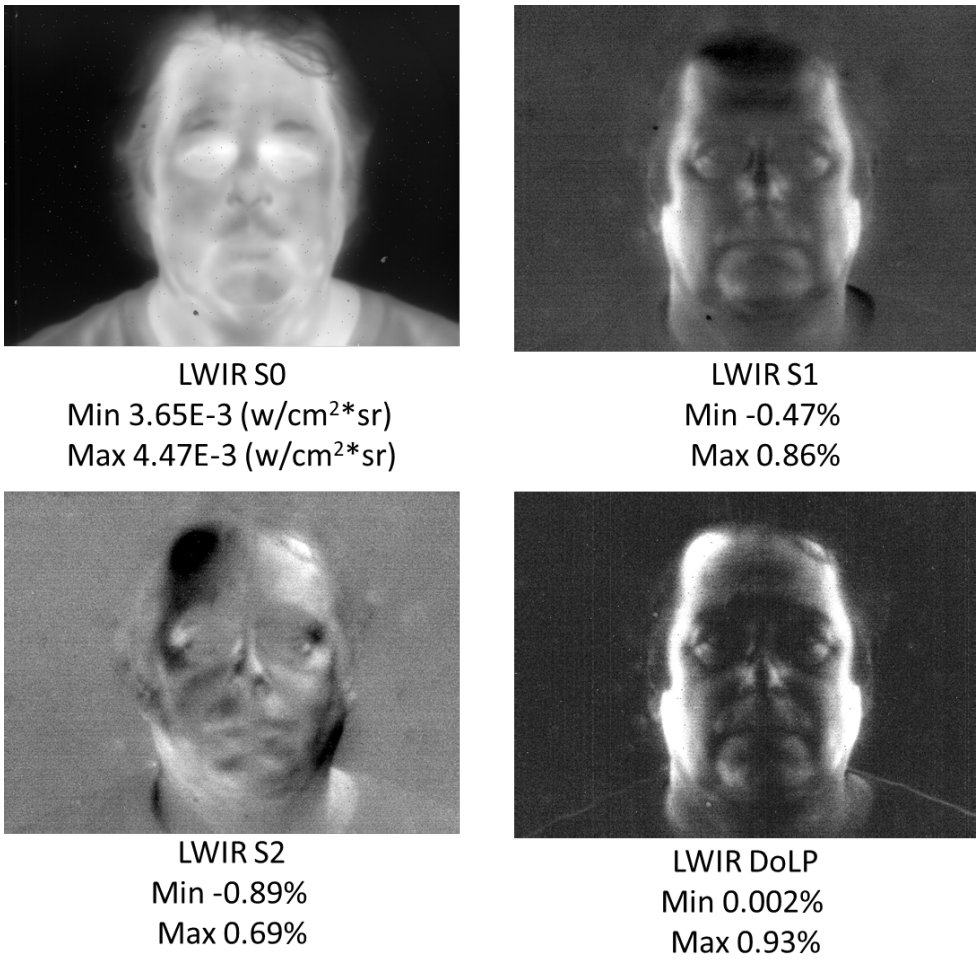

Fig. 17 LWIR image set recorded indoors of human subject at body temperature T = 36 °C. Shown are S0, S1, S2 and DoLP imagery. Displayed below each image are the minimum and maximum pixel values based on an ROI similar to what is shown in Fig. 10.

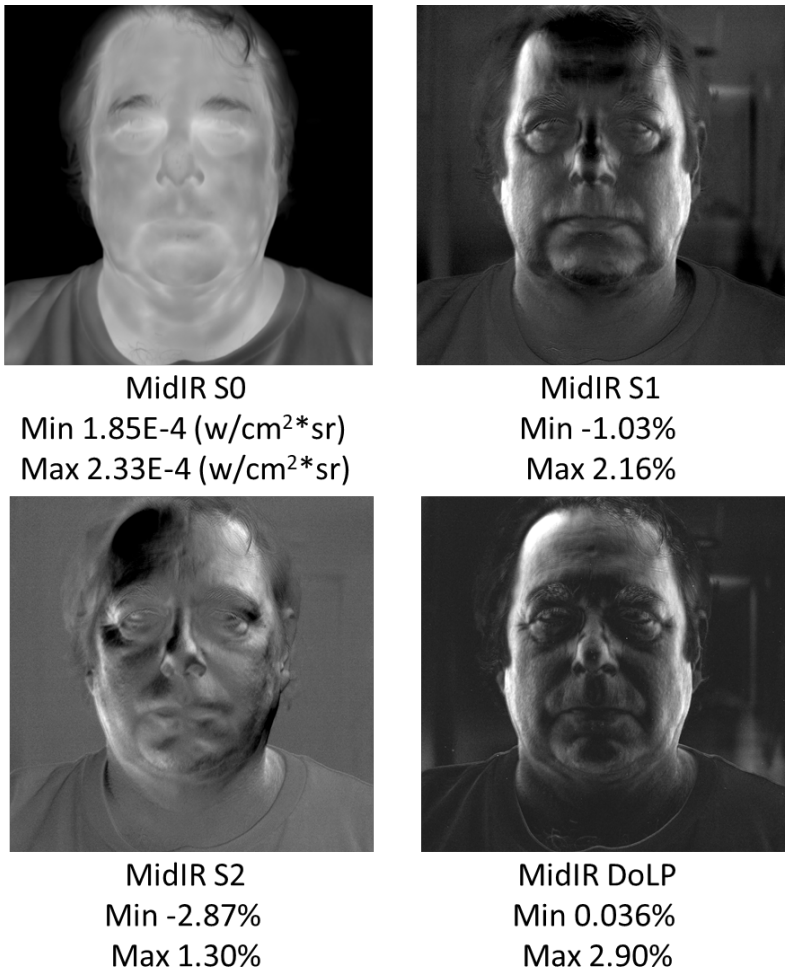

Fig. 18 MidIR image set recorded indoors of human subject at body temperature T = 36 °C. Shown are S0, S1, S2 and DoLP imagery. Displayed below each image are the minimum and maximum pixel values based on an ROI similar to what is shown in Fig. 10.

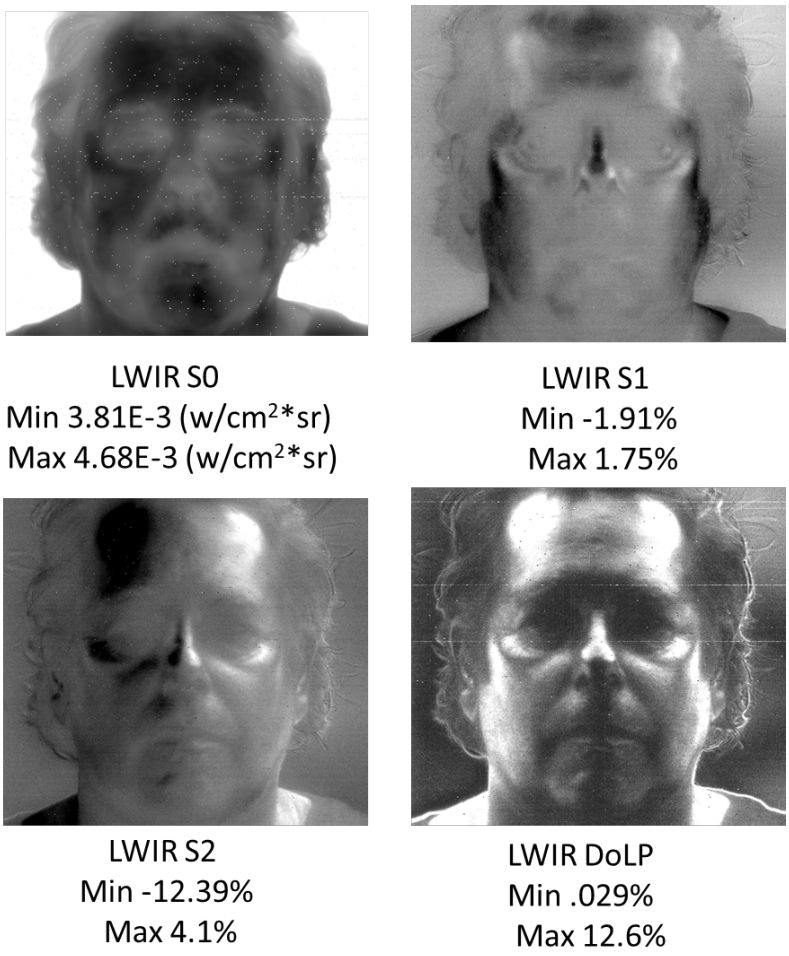

Fig. 19 LWIR image set of a human subject recorded outside under direct sunlight and hot atmospheric conditions (i.e., 36–37 °C [97–98 °F]). As a result, measured skin temperature was slightly elevated to T = 37 °C. Displayed below each image are minimum and maximum pixel values for S0, S1, S2, and the DoLP image based on an ROI similar to what is shown in Fig. 10.

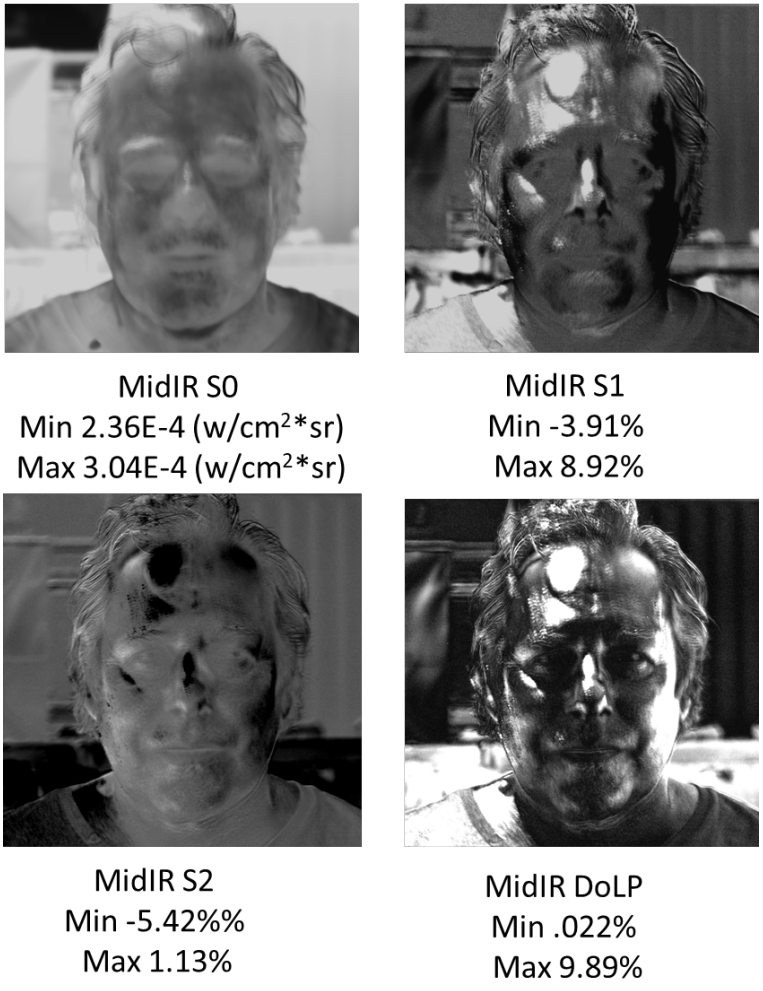

Fig. 20 MidIR image set of a human subject recorded outside under direct sunlight and hot atmospheric conditions (i.e., 36–37 °C [97–98 °F]). As a result, measured skin temperature was slightly elevated to T = 37 °C. Displayed below each image are minimum and maximum pixel values for S0, S1, S2, and the DoLP image based on an ROI similar to what is shown in Fig. 10.

For subjects recorded outdoors, the amount of ambient radiance in the LWIR is reduced and emission-induced polarization is dominate compared to the reflection-induced polarization, resulting in a higher measured DoLP in the LWIR. This effect is clearly seen by comparing the two DoLP images shown in Figs. 17 and 19 in which the measured maximum DoLP are 0.93% and 12.6%, recorded inside and outside, respectively.

The comparison between the LWIR and MidIR image sets shown in Figs. 19 and 20 recorded outside displays somewhat different behavior in relation to the measured DoLP values as seen in the manikin set. Unlike the manikin set, in which the measure maximum DoLP was greater for the MidIR image compared to the LWIR image, here, for the human subject, the measured DoLP recorded in the

LWIR is larger than that seen in the MidIR DoLP image (i.e., 12.6% for the LWIR comparted to 9.60% for the MidIR image). This is believed to be a direct result of chemical and tactile differences between the manikin head and the human subject. Specifically, the manikin was coated with a "diffuse" carbon-black pigment, while the human subject (who was exposed to usually hot and humid conditions during the test period) exhibited a degree of perspiration that resulted in an optical smooth skin surface. It is worth noting how naturally occurring skin oil and perspiration affect the MidIR thermal S0 and corresponding polarimetric images shown in Fig. 20, highlighted the obvious region of high polarization located on one side of the forehead. This undoubtable is a result of induced polarization due to strong specular reflection of the sun radiance in the MidIR waveband. However, this effect is not as apparent in the LWIR, since the magnitude of solar radiance in the LWIR is more than an order of magnitude lower.[22]

6. Conclusion

The ability record imagery appropriate for human ID in environments in which no visible illumination is present is an ability required for robust nighttime surveillance. Prior research involving thermal polarimetric imaging showed that such ability may be possible, but were limited to imagery recorded only in the LWIR. Research in the LWIR reported that performance was modestly affected by the location in which the human subject was imaged (i.e., indoors versus outdoors). Variation in the polarimetric response was attributed to differences in the magnitude ambient radiance levels in the LWIR depending on outside or indoor operation. It was suggested that such effects might be mitigated by conducting polarimetric imaging in the MidIR portion of the spectrum where ambient levels are lower.

Presented here is a study designed to help address this question in which MidIR polarimetric imagery of facial profiles are recorded and compared to a corresponding set of imagery recorded in the LWIR. Test subjects were recorded for both indoor and outdoor settings, using a human subject and a pair of artificially coated manikin heads to mimic reflective and emissive surfaces.

Polarimetric response was measured as a function of temperature in both the MidIR and LWIR bands for reflective and emissive surfaces. Results of the temperature-dependent study shown in Fig. 7 show a plateauing in polarization response with increasing temperature. This effect results when the fraction of ambient radiance in the imaging environment becomes exceedingly small when compared to the ever-increasing degree of thermal emission that results due to rising temperatures (i.e., polarization due to emission becomes greater than polarization due to reflection).

Results comparing polarimetric response for reflective- and emissive-surfaced manikin heads conducted indoors, showed, in general, better performance for operation in the MidIR compared to the LWIR, even when adjustments are made for the differencing radiometric and FPA technologies. This apparent advantage of MidIR compared to LWIR polarimetric imaging was again demonstrated when subjects were imaged outside. This was particularly notable since in theory, polarimetric performance in the LWIR should have benefited more (compared to the MidIR) by operating in a low ambient environment. Finally, it should be noted this comparison of MidIR versus LWIR polarimetric image performance was far from ideal, due to significant differences in camera design and components used in the development of each system. This problem is expected be rectified in the near future when a new dual-band MidIR/LWIR polarimetric platform is received. A more accurate quantitative comparison between the two bands is expected since the new dual-band camera system is expected to share an identical optical train, imaging objectives, and other important components.

7. References

1. Kudenov M, Pezzaniti L, Grant G. Microbolometer-infrared imaging Stokes polarimeter. Optical Eng. 2009 June;48(6).

2. Pezzaniti JL, Chenault DB. A division of aperture MWIR imaging polarimeter. Proc. SPIE 5888. 2005;58880V.

3. Farlow CA, Chenault DB, Spradley KD, Gulley MG, Jones MW, Persons CM. Imaging polarimeter development and application. In: DH Goldstein, DB Chenault, W Egan and MJ Duggin, editors. Polarization analysis and measurement IV, Proc. SPIE 4819. 2001;118–125.

4. Bowers D, Boger JK, Wellens LD, Black WT, Ortega SE, Ratliff BM, Fetrow MP, Hubbs JE, Tyo JS. Evaluation and display of polarimetric image data using long-wave cooled micro-grid focal plane arrays. In: DH Goldstein and DB Chenault, eds. Proc. SPIE vol. 6240: Polarization: Measurement, Analysis, and Remote Sensing VII, SPIE. 2006:6240OF.

5. Gurton KP, Felton M. Detection of disturbed earth using passive LWIR polarimetric imaging. Proceedings of the SPIE Optics and Photonics Conference; 2009 Aug 2–6; San Diego, CA.

6. An C, Grantham J, King J, Robinson J, Pezzaniti L, Gurton K. Utility of polarization sensors for clutter rejection. 6th Annual US Missile Defense Conference; 2008 Mar 31–Apr 3.

7. Gurton KP, Felton M. Detection of buried improvised explosive devices (IED) using passive long-wave infrared (LWIR) polarimetric imaging. Army Research Laboratory (US); 2009 Sep. Report No.: ARL-TR-4941.

8. Harchanko JS, Chenault DB, Farlow CF, Spradley K. Detecting a surface swimmer using long wave infrared imaging polarimetry. In: MJ DeWeert and TT Saito, editors. Photonics for port and harbor security. Proc SPIE 5780. 2005.

9. Hu S, Short N, Gurton K, Riggan B. Overview of polarimetric thermal imaging for biometrics. Polarization: Measurement, Analysis, and Remote Sensing XIII SPIE Commercial & Scientific Imaging; 2018 Apr 15–19.

10. Hu S, Short N, Gurton K, Riggan B. A polarimetric thermal database for face recognition research. IEEE Conference on Computer Vision and Pattern Recognition; 2016 June 26–July 1.

11. Shuowen S, Short N, Gurton K, Riggan B. Polarimetric thermal based face recognition. Polarization, Measurement, Analysis, and Remote Sensing XII, SPIE Defense & Commercial Sensing Symposia; 2016 Apr 17–24.

12. Hu S, Short N, Gurton K. Exploiting polarization-state information for cross-spectrum face recognition. 2015 IEEE 7th International Conference on Biometrics Theory, Applications and Systems (BTAS); 2015 Sep 8–11.

13. Hu S, Short N, Gurton K, Gurram P, Reale C. MWIR-to-visible and LWIR-to-visible face recognition using partial least squares and dictionary learning. In: Bourlai T, editor. Face recognition across the electromagnetic spectrum. Springer Press; 2015.

14. Short N, Hu S, Gurram P, Gurton K, Chan A. Improving cross-modal face recognition using polarimetric imaging. Optics Letters. 2015;40(6):882–885.

15. Yufa A, Gurton K, Videen G. Three-dimensional (3D) facial recognition using passive LWIR polarimetric imaging. Appl Opt. 2014 Dec;53(36):8514–8521.

16. Gurton K, Yuffa A, Videen G. LWIR Polarimetry for enhanced facial recognition in thermal imagery. Proceedings of SPIE 9099, Polarization: Measurement, Analysis, and Remote Sensing XI; 2014 May 21.

17. Gurton KP, Yuffa A, Videen G. Enhanced facial recognition for thermal imagery using polarimetric imaging. Opt Lett. 2014;39(13):3857–3859.

18. Gurton KP, Felton M, Pezzaniti L. Remote detection of buried land-mines and IEDs using LWIR polarimetric imaging. Optics Express. 2012;20(20):22344–22359.

19. Gurton KP, Felton MA, Mack R, Farlow C, Pezzaniti L, Kudenov MW, LeMaster D. MidIR and LWIR polarimetric sensor comparison study., In: Polarization: Measurement, Analysis, and Remote Sensing IX; 2010; Orlando, FL. Proc SPIE. 2010;7672.

20. Hecht E, Zajac A. Optics. Addison-Wesley Publishing; 1979.

21. Siegel R, Howel J. Thermal radiation heat transfer. McGraw-Hill Publishing; 1981.

22. Felton M, Gurton K, Pezzaniti L. Measured comparison of the crossover periods for mid- and long-wave IR (MWIR and LWIR) polarimetric and conventional thermal imagery. Optics Express. 2010;18(15):15704–15713.

23. Charlton M, Stanley S, Whitman Z. The effect of constitutive pigmentation on the measures emissivity of human skin. Journal PONE. 2020;15(11).

24. Wolfe WL, Zissis GJ. The infrared handbook. Environmental Research Institute of Michigan Press; 1978.

25. Gurton K, Dahmani R, Videen G. Effect of surface roughness and complex indices of refraction on polarized thermal emission. Appl Opt. 2005 Sep;44(26).

List of Symbols, Abbreviations, and Acronyms

2-D	two-dimensional
DoA	division-of-amplitude
DoLP	degree-of-linear-polarization
EM	electromagnetic
FOV	field of view
FPA	focal-plane array
ID	identification
IED	improvised explosive device
InSb	indium antimonide
IR	infrared
LWIR	longwave infrared
MCT	mercury cadmium telluride
MidIR	mid-IR
NIR	near-IR
NUC	non uniformity correction
ROI	region of interest
SAR	spinning achromatic retarder
SWIR	shortwave IR

1 (PDF)	DEFENSE TECHNICAL INFORMATION CTR DTIC OCA
1 (PDF)	DEVCOM ARL FCDD RLD DCI TECH LIB
1 (PDF)	DEVCOM ARL FCDD RLC ES K GURTON